

## Preparation and Characterization of 49% Poly(Methyl Methacrylate) Grafted Natural Rubber (MG49)–Stannum (IV) Oxide (SnO<sub>2</sub>)–Lithium Salt Based Composite Polymer Electrolyte

A. Ahmad<sup>1,2,\*</sup>, M.Y.A. Rahman<sup>3,\*</sup>, H. Harun<sup>1,2</sup>, M.S. Su'ait<sup>1,2</sup>, M.A. Yarmo<sup>2</sup>

<sup>1</sup> Polymer Research Center, Faculty of Science and Technology, Universiti Kebangsaan Malaysia, 43600 Bangi, Selangor, Malaysia.

<sup>2</sup> School of Chemical Sciences and Food Technology, Faculty of Science and Technology, Universiti Kebangsaan Malaysia, 43600 Bangi, Selangor, Malaysia.

<sup>3</sup> College of Engineering, Universiti Tenaga Nasional, 43009 Kajang, Selangor, Malaysia.

\*E-mail: [yusri@uniten.edu.my](mailto:yusri@uniten.edu.my); [azizan@ukm.my](mailto:azizan@ukm.my)

Received: 21 June 2012 / Accepted: 31 July 2012 / Published: 1 September 2012

---

49% poly(methyl methacrylate) grafted natural rubber (MG49) in the presence of 4% wt. stannum (IV) oxide (SnO<sub>2</sub>) and lithium salts (lithium tetrafluoroborate, LiBF<sub>4</sub> and lithium perchlorate, LiClO<sub>4</sub>) in composite polymer electrolyte (CPE) films has been prepared. The MG49-SnO<sub>2</sub> polymer electrolyte films were prepared via solution casting technique at different concentrations ranging from 0% wt. to 30% wt. The effect of the lithium salt concentration based on morphological observation, structural, chemical interaction and ionic conductivity studies of MG49-SnO<sub>2</sub> composite polymer electrolytes film have been studied. Morphological observation showed that SnO<sub>2</sub> nanoparticles were well dispersed in MG49 films. The addition of lithium salts has changed the topological texture from a smooth and dark surface to a rough and bright surface. The structural observation showed that complexation and re-crystallization have occurred in the system. FTIR and XPS analysis confirmed that some interaction between lithium ion and oxygen atoms were observed at the carbonyl (C=O) (1730 cm<sup>-1</sup>-1710 cm<sup>-1</sup>) and ether group (C-O-C) (1300 cm<sup>-1</sup>-950 cm<sup>-1</sup>). The highest ionic conductivity was given by 30% wt. LiBF<sub>4</sub> at  $1.6 \times 10^{-6}$  S cm<sup>-1</sup> in comparison to LiClO<sub>4</sub> was  $6.0 \times 10^{-8}$  S cm<sup>-1</sup> at 20% wt.. The conductivity of MG49-SnO<sub>2</sub>-LiClO<sub>4</sub> obeys the Arrhenius equation in temperature range from 303 to 373 K with the pre-exponential factor,  $\sigma_0$  of  $5.33 \times 10^{-2}$  S cm<sup>-1</sup> and the activation energy,  $E_a$  of 0.25 eV. On the other hand, MG49-SnO<sub>2</sub>-LiBF<sub>4</sub> exhibited non-Arrhenius-like behaviour at the same temperature range. The electrochemical stability of MG49-SnO<sub>2</sub>-LiClO<sub>4</sub> has been found to maintain its shape even after the 100<sup>th</sup> cycle in the range of -2.0 to +2.2 mV and -8.0 to +6.0 mV for MG49-SnO<sub>2</sub>-LiBF<sub>4</sub>.

---

**Keywords:** 49% poly(methyl methacrylate) grafted natural rubber (MG49), Composite polymer electrolyte, Ionic conductivity, Infrared analysis, Stannum (IV) oxide (SnO<sub>2</sub>),

## 1. INTRODUCTION

The breakthrough of ionic conducting materials in solid polymer material complexes with salt by Fenton et. al in 1973 [1] has led to the development of electrochemical devices application [2]. Recently, modified natural rubber such as epoxidised natural rubber (ENR) and poly (methyl methacrylate) (PMMA) grafted natural rubber (MG) based polymer electrolytes had drawn the attention of many researches [3-16]. Modified natural rubber such as ENR 25, ENR 50, MG30 and MG49 has oxygen atom at PMMA segment that can act as electron donor atoms in the polymeric structure. The oxygen atom with lone pair of electron forms a coordinate bond with cation from metal salts, resulting in the formation of polymer-complexes [3-6]. Modified natural rubber has attractive attributes such as soft elastomer characteristic at room temperature and good elasticity. A suitable elasticity can result in a flat and flexible film. Therefore, a good interfacial contact is expected between electrolyte and electrode in electrochemical devices. However, ENR film shows disadvantages in terms of its mechanical properties such as slightly sticky and difficulty to peel off from substrate [5,7-10]. Moreover, modified natural rubber has low glass transition temperature ( $T_g$ ) ENR =  $-25\text{ }^\circ\text{C}$ , MG49 =  $-60\text{ }^\circ\text{C}$  that promotes a more amorphous phase for segmental motion. MG49 was selected because 49% is the highest percentage of PMMA grafted on natural rubber backbone. Previous works on various MG based polymer electrolytes were conducted elsewhere [3,4,6,7,11-16].

The smaller cation size of lithium ion could contribute to ion dissociation that resulted from coulombic interaction forces between the two oppositely charged ions and the thermodynamic interactions between solvent and solute molecules in aprotic solvent [20]. Other factors such as cation polarity and large anion size are required for delocalization of ionic charge that could minimize the lattice energy value [2]. Lithium salts are being added in the polymer electrolyte systems because of the Lewis acid behaviours. Therefore, lithium salt can interact with electron donor centres. Other works [21,22] reported that  $\text{LiClO}_4$  salt is very stable at ambient moisture and is less hygroscopic in comparison to  $\text{LiCF}_3\text{SO}_3$  salt. However, the high oxidation state of chlorine (VII) in perchlorate makes it a strong oxidant that readily reacts with most organic species in violent ways under certain conditions such as high temperature and high current charge [22]. On the other hand,  $\text{LiBF}_4$  is a salt based on an inorganic super-acid anion and is less toxic in comparison to  $\text{LiAsF}_6$  and  $\text{LiClO}_4$  [23].

The introduction of inert filler such as titania ( $\text{TiO}_2$ ), alumina ( $\text{Al}_2\text{O}_3$ ), silica ( $\text{SiO}_2$ ), zirconia ( $\text{ZrO}_2$ ) and stannum oxide ( $\text{SnO}_2$ ) has been proven to increase the ionic conductivity value by weakening the polymer-salts interactions [16-19]. However, sufficient number of works were carried out on modified rubber based composite polymer electrolyte in order to improve the conductivity [10,15,16,25]. One of the successful studies was carried out by Low et al. [15,16] whereby several of  $\text{TiO}_2$  concentrations were incorporated via *in-situ* sol-gel in modified rubber, MG49, giving a high ionic conductivity at  $\sim 10^{-5}$   $\sim 10^{-3}$   $\text{S cm}^{-1}$ .

In this work, composite polymer MG49- $\text{SnO}_2$  (4% wt.) was doped with 0% wt. to 30% wt. lithium salts ( $\text{LiBF}_4$  and  $\text{LiClO}_4$ ) to prepare composite polymer electrolytes (CPE) via solution casting technique. All of the samples were characterized by using scanning electron microscopy-energy dispersive X-ray spectroscopy (SEM-EDX), X-ray diffraction (XRD), attenuated total reflection-Fourier transform-infrared (ATR-FTIR), X-ray photoelectron spectrometer (XPS), AC electrochemical

impedances spectroscopy (EIS) and cyclic voltammetry (CV). It was expected that an optimum quantity of lithium salt raises the conductivity in composite polymer MG49-SnO<sub>2</sub>, giving an appropriate difference between LiBF<sub>4</sub> and LiClO<sub>4</sub> salts.

## 2. MATERIALS AND METHODS

### 2.1 Materials

MG49 was obtained under the commercial name “MEGAPOLY” from Green HPSP (Malaysia) Sdn. Bhd., Petaling Jaya, Malaysia. SnO<sub>2</sub> was supplied by Sigma-Aldrich. LiClO<sub>4</sub> and LiBF<sub>4</sub> salts were supplied by Fluka Chemicals, Germany. Organic solvents such as toluene and tetrahydrofuran (THF) were supplied by System ChemAR, Poland. All materials were used without further purification.

### 2.2 Sample preparation

Samples were prepared by solution casting technique. 3 g of MG49 was dissolved in 75 mL toluene. After 24 hours, the solution was stirred with efficient magnetic stirring for the next 24 hours until complete dissolution of MG49 solution was achieved. 0% wt. to 30% wt. of LiClO<sub>4</sub> salt was dissolved separately in 10 mL THF solution and was added into the solution for the next 24 hours under continuous stirring. 4% wt. SnO<sub>2</sub> then mixed for the next 24 hours to obtain a homogenous solution. 20 mL electrolyte solution was then casted onto a glass petri dish and the solvent were allowed to slowly evaporate at room temperature. Residual solvent was then removed by drying the polymer in a vacuum oven for 24 hours at 50 °C. The samples were then stored in a dry storage cabinet at 30% humidity until further use. The same experimental procedure was repeated with different weight percentage of LiBF<sub>4</sub> salt.

### 2.3 Characterization

The surface morphology of the samples was observed using SEM model LEO 1450 VP, Carl Zeiss, together with EDX, Oxford Instrument at 2000× magnification and 15 kV electron beam. The sample was fractured in liquid nitrogen and coated with gold sputtered-coated machine before the analysis. XRD model D8 Advance, Bruker was performed to observe the crystallinity with the presence of lithium salts. The data were collected from the range of diffraction angle  $2\theta$  from 10° to 60° at a scanning rate 0.04° s<sup>-1</sup>. FT-IR spectrum was recorded by computer interfaced with ATR-FTIR Perkin Elmer Spectrum 2000 Spectrometer. The electrolyte films were placed onto KBr windows and were analyzed in the frequency range of 4000 cm<sup>-1</sup> to 400 cm<sup>-1</sup> with a scanning resolution of 4 cm<sup>-1</sup>. XPS spectra were obtained from XPS model Axis Ultra DLD, Kratos/Shimadzu by irradiating the electrolyte films with monochromatic Al K $\alpha$  of X-rays beams while simultaneously measuring the binding energy and number of electrons that escape from the top of the electrolyte films. The

binding energy at 284.5 eV for C 1s has been used for calibration and charging effect correction. The based pressure of this instrument was setup at  $10^{-10}$  torr. The ionic conductivity measurements were carried out by EIS, Solartron Schlumberger SI 1286 using high frequency resonance analyzer (HFRA) model 1255 with applied frequency from 1 MHz to 0.1 Hz at room temperature. The conductivity measurements were conducted at room temperature at a temperature range of 303 K to 373 K. The 16 mm in diameter disc-shaped sample was sandwiched between two stainless steel block electrodes. Cyclic voltammetry was performed using potentiostats model reference 600 with PHE200 physical electrochemistry software provided by Gamry instrument to determine the cyclability of the electrolyte. The sample was sandwiched between the symmetrical stainless steel (SS) electrodes. The voltammogram was recorded for 100 cycles at a scan rate of  $5 \text{ mV s}^{-1}$  in the range of  $-1.5$  and  $+1.5 \text{ V}$ . The analysis was performed at room temperature.

### 3. RESULTS AND DISCUSSION

#### 3.1 Morphology Studies

Morphology studies were carried out using SEM to observe the effect of lithium salts concentration on the fractured surface of the MG49-SnO<sub>2</sub>. Fig. 1 shows the SEM micrograph of MG49-SnO<sub>2</sub> with EDX spectra at 15,000× magnification. The EDX spectra confirmed the existence of stannum and oxygen elements in the system. Meanwhile, SEM micrograph indicated that the compound have smooth surface with some SnO<sub>2</sub> nanoparticles dispersed in the matrix with the average sizes of ~100 nm.

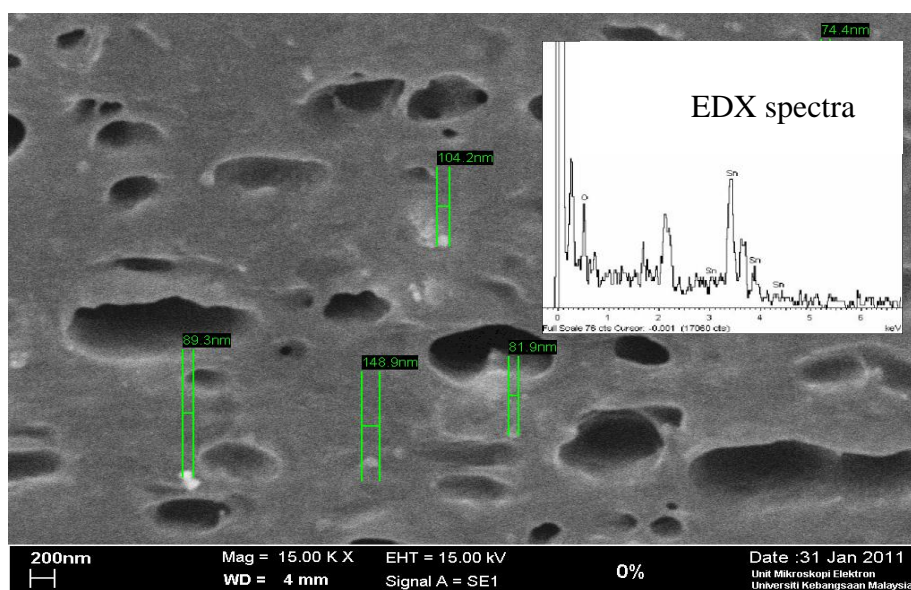


**Figure 1.** SEM micrograph and EDX spectra of MG49-SnO<sub>2</sub>

Fig. 2 shows the SEM micrograph of MG49 (a) pure (b) with 4% wt. SnO<sub>2</sub> and MG49-SnO<sub>2</sub> with (c) 20% wt. LiClO<sub>4</sub> (d) 30% wt. LiClO<sub>4</sub> (e) 20% wt. LiBF<sub>4</sub> (f) 30% wt. LiBF<sub>4</sub>. SEM micrograph in Fig. 2 (a) shows a homogenous surface of rubber based film using solution blending technique. The flexibility and elasticity properties of the rubber based film were attributed by the polyisoprene soft segment in MG49, while the hard segment was contributed by the PMMA that has been grafted onto rubber chain [25].

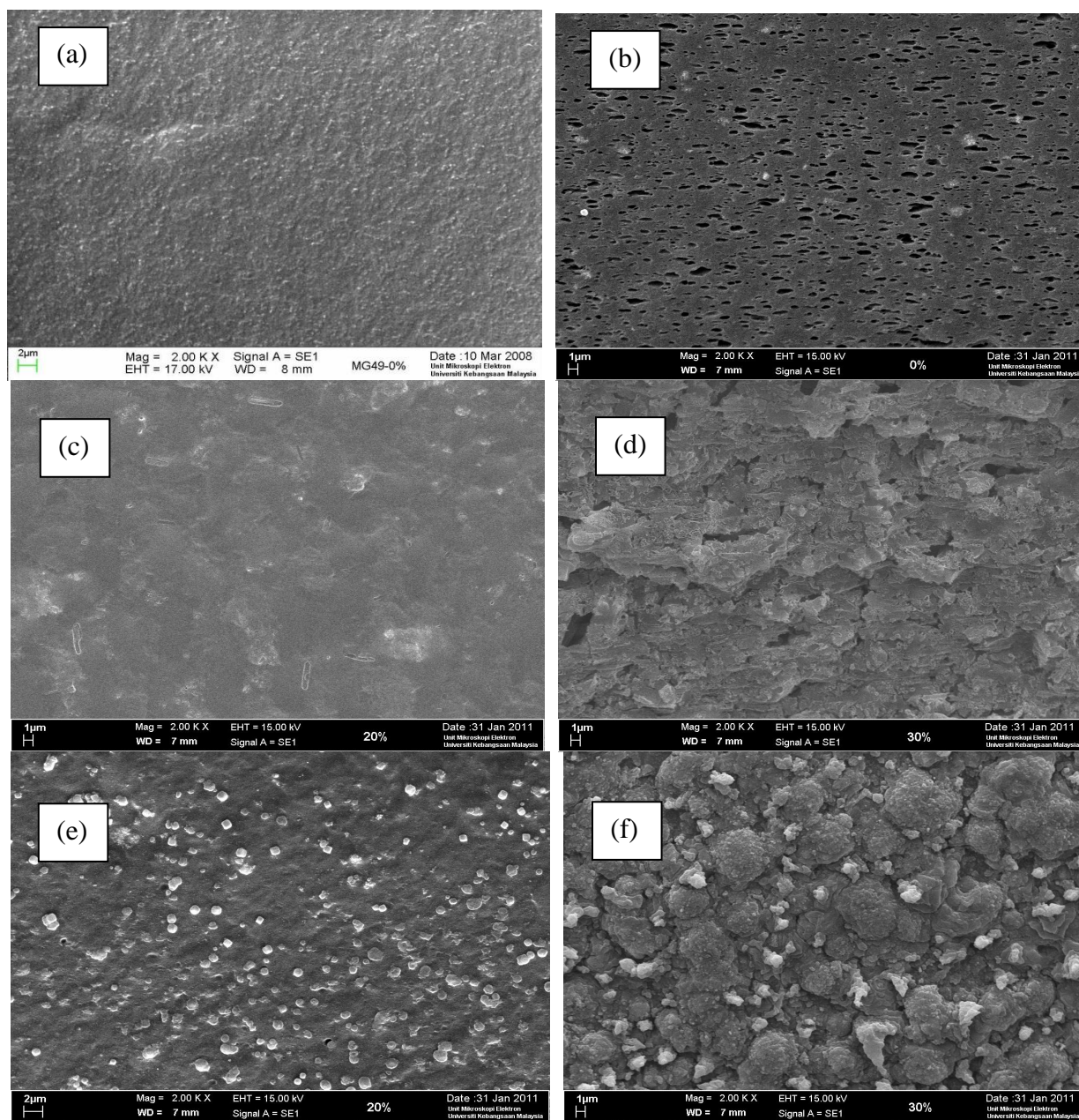


**Figure 2.** SEM micrograph of (a) pure MG49 (b) MG49-SnO<sub>2</sub> (4% wt.) and MG49-SnO<sub>2</sub> with (c) 20% wt. LiClO<sub>4</sub> (d) 30% wt. LiClO<sub>4</sub> (e) 20% wt. LiBF<sub>4</sub> (f) 30% wt. LiBF<sub>4</sub>

The observation on Fig. 2 (b) shows rubber based film surfaces with the presence of bright spot indicated that SnO<sub>2</sub> nanoparticles is presence as confirmed by EDX spectra in Fig. 1. Morphological

observation shows that SnO<sub>2</sub> nanoparticles were well dispersed in MG49 matrix but not compatible and miscible with MG49 host. The cross-sectional view of this film also shows the formation of micropores due to the interaction between the solvent and polymer host, as reported by Ahmad and co-workers [25].

The topological textures of MG49 have changed from smooth and dark fractured surface to rough and brighter surface after the addition of lithium salt. Monikowska et al. [27] suggested that dark region in the SEM micrograph signifying an amorphous phase. In this work, the dark region was contributed by rubber chain that shows amorphous phase. Further additions of lithium salt in this system will lead to the re-crystallization of lithium salt because of high salt concentration in the electrolyte system. The high salt concentration gives a high tendency to the ionic species to associate or aggregate with each other [13, 28-30]. This will decrease the number of the conducting species and decreases the ionic mobility due to ionic migration in the segmental polymer chain. This process will disturb the conducting process in the electrolyte systems and provide a low conductivity in the systems [6]. The presence of high crystalline phase are confirmed by XRD patterns shown in Fig. 3.

### 3.2 XRD studies

The XRD analysis is performed to determine the structure and crystallization of polymer-salts complex. The reduction in semi-crystalline phase of electrolyte improves the conductivity as reported elsewhere [2,8,31-35]. Fig. 3 (a) shows the XRD patterns of MG49-SnO<sub>2</sub>-LiClO<sub>4</sub>. Meanwhile, Fig. 3 (b) shows the XRD patterns of MG49-SnO<sub>2</sub>-LiBF<sub>4</sub>. Pure SnO<sub>2</sub> shows high intense peak at  $2\theta$ , 26.5° (110), 33.8° (101), 37.9° (200) and 51.8° (211). All of the peaks can be indexed to tetragonal rutile SnO<sub>2</sub> structure (JCPDS card no. 41-1445). The same broad peaks characteristics of a rutile phase of SnO<sub>2</sub>, indicating a formation of a rutile lattice structure, similar to observations done by Stefanov et al. [36] and Li et al. [37]. Pure LiClO<sub>4</sub> shows high intense peak at  $2\theta$ , 12.1°, 13.5°, 21.1°, 23.3°, 31.7°, 33.1°, 35.7°, 39.5°, 47.3°, 49.3°, 52.3° and 58.0° in Fig. 3 (a). While, pure LiBF<sub>4</sub> peaks were observed at  $2\theta$ , 13.5°, 18.8°, 21.5°, 23.6°, 26.8°, 28.2°, 32.0°, 32.8°, 39.9°, 44.6° and 54.9° in Fig. 3 (a). The introduction of SnO<sub>2</sub> nanoparticles to the polymer host were found to increase the semi-crystalline phase of PMMA grafted natural rubber by increasing hump in the region between 10° to 20°. Moreover, all SnO<sub>2</sub> intensity peak at  $2\theta$ , 26.5°, 33.8°, 37.9° and 51.8° were increased drastically upon the addition of SnO<sub>2</sub> nanoparticles. After the addition of lithium salt, the crystallinity was found to increase via the increase of lithium salts concentration. The presence of high intense peaks at the high salt concentration for LiClO<sub>4</sub> and LiBF<sub>4</sub> are around the angles of  $2\theta$ , 13.5°, 23.3°, 31.7°, 35.7°, 39.5° and at  $2\theta$ , 21.5°, 28.2°, 39.9° respectively, indicating that the re-crystallization occurs in the polymer host. The re-crystallization of lithium salts was due to the ion association between Li<sup>+</sup> cations and anions in the electrolyte at the high salt concentration [12]. This finding was similar to those reported elsewhere whereby the ionic conductivity was improved by the reduction of crystalline phase or the enhancement of amorphous phase in the polymer host [2,12,31-35].

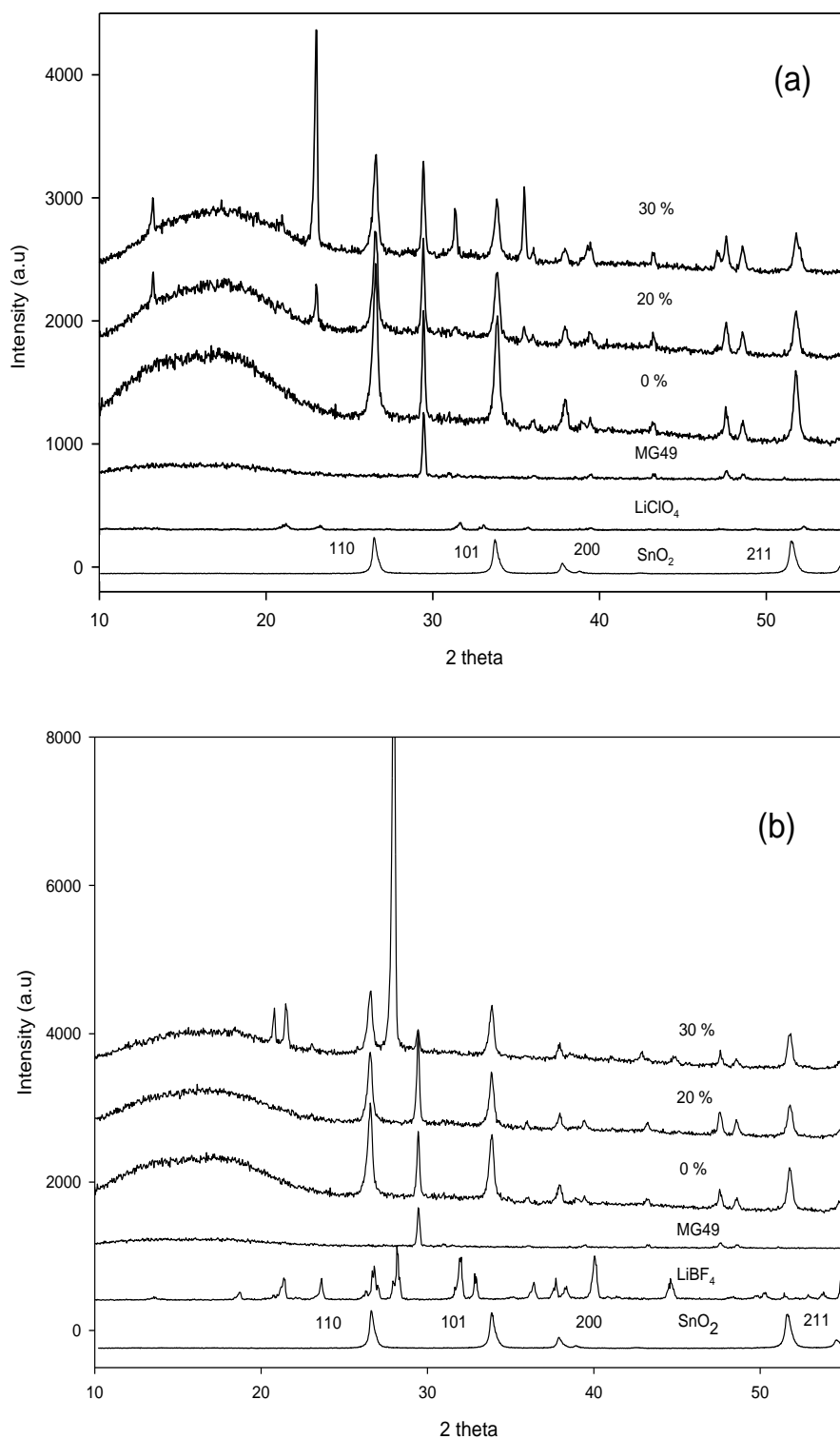


**Figure 3.** XRD pattern of (a) MG49-SnO<sub>2</sub>-LiClO<sub>4</sub> and (b) MG49-SnO<sub>2</sub>-LiBF<sub>4</sub>

### 3.3 FT-IR Analysis

Since each type of covalent bonds has a different natural frequency of energy vibration, the identification of absorption peak in the vibration portion of infrared region will give a specific type of

covalent bonding [38]. The main interests are on the oxygen atoms of the carbonyl ( $\text{C}=\text{O}$ ) ( $1750\text{ cm}^{-1}$ - $1730\text{ cm}^{-1}$ ) and ether group ( $\text{C}-\text{O}-\text{C}$ ) ( $1300\text{ cm}^{-1}$ - $1000\text{ cm}^{-1}$ ) in MG49. According to the literature, the oxygen atoms in the structure of polymer host acted as electron donor atoms and formed a coordinate bond with lithium ion from doping salts to form polymer-metal salt complexes [3,4,21,25,31-34]. The vibration frequency of polymer-metal salt complexes was shifted to lower wavenumbers by about  $15\text{ cm}^{-1}$  to  $25\text{ cm}^{-1}$  in comparison to their polymer host [38].

Fig. 4 (a) and (b) demonstrates the FT-IR spectrum of symmetrical stretching of carbonyl group,  $\nu(\text{C}=\text{O})$  in MG49 for  $\text{LiClO}_4$  and  $\text{LiBF}_4$ , respectively. The vibration of  $\nu(\text{C}=\text{O})$  in MG49 and MG49 with the presence of 4% wt.  $\text{SnO}_2$  give rise to an intense, sharp and very strong peak at  $1727\text{ cm}^{-1}$ . There is no peak shift between MG49 polymer host and  $\text{SnO}_2$  nanoparticles, indicating that there is no chemical interaction occurred. However, the peak intensity in the region of  $1700\text{ cm}^{-1}$  to  $1600\text{ cm}^{-1}$  is increased with the addition of  $\text{SnO}_2$  nanoparticles. With the addition of lithium salts for  $\text{LiClO}_4$  and  $\text{LiBF}_4$ , the peak intensity of  $\nu(\text{C}=\text{O})$  of MG49 is shifted from  $1727\text{ cm}^{-1}$  to lower wavenumbers,  $1717\text{ cm}^{-1}$  and  $1718\text{ cm}^{-1}$ , respectively. Moreover, the peak intensity in this region became sharper as the concentration of lithium salts increased.

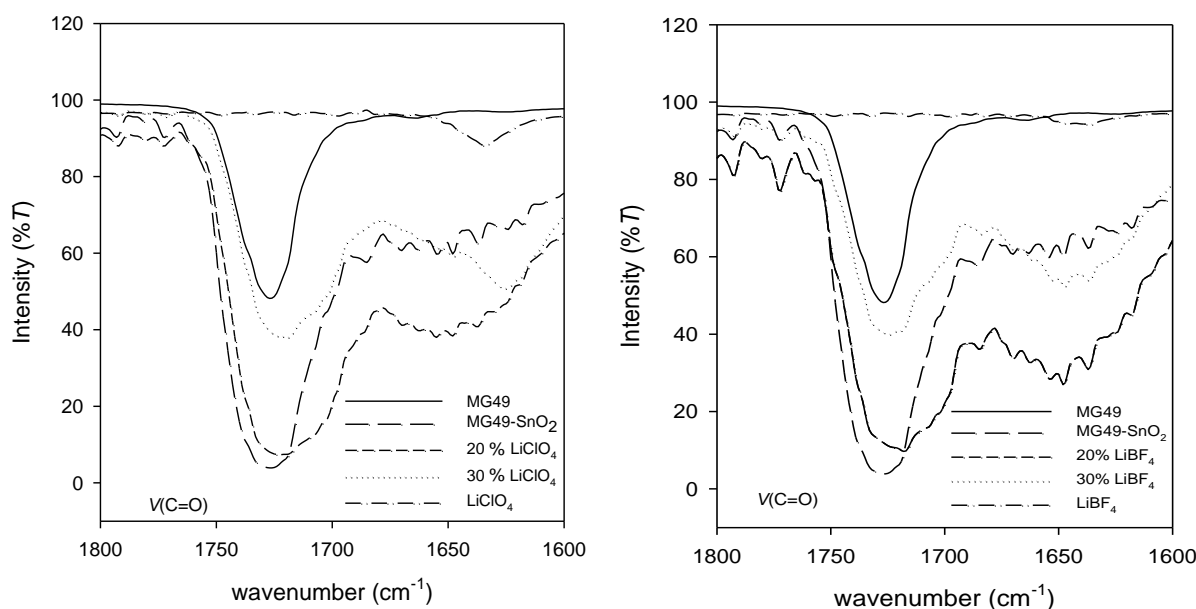


**Figure 4.** FT-IR spectrum of symmetrical stretching of carbonyl group,  $\nu(\text{C}=\text{O})$  (a)  $\text{LiClO}_4$  and (b)  $\text{LiBF}_4$

This behaviour indicated that a certain amount of lithium salt was able to interact with polymer matrix and limits the number of lithium ion for coordination [9,10]. The specific vibration mode of ether group ( $\text{C}-\text{O}-\text{C}$ ) for MG49 in Fig. 5 (a) and (b) can be observed at symmetrical stretching mode,  $\nu_s(\text{C}-\text{O}-\text{C})$ , stretching mode of  $-\text{COO}-$ ,  $\nu(\text{C}-\text{O})$ , asymmetrical stretching mode,  $\nu_{as}(\text{C}-\text{O}-\text{C})$ , and asymmetric deformation of the PMMA,  $\delta(\text{O}-\text{CH}_3)$  [6]. However, there is no significant peak shifting observed at asymmetric deformation of the PMMA,  $\delta(\text{O}-\text{CH}_3)$  at  $1447\text{ cm}^{-1}$ . The entire specific

vibration mode of ether group (C-O-C) in MG49 is not shifted after the addition of 4% wt. SnO<sub>2</sub> nanoparticles. This signifies that there is no chemical interaction occurred between MG49 with SnO<sub>2</sub> nanoparticles. Moreover, two main peaks at 660 and 560 cm<sup>-1</sup> that are ascribed to the Sn-O vibrations of the Sn-O-Sn and the Sn-O-H bonds are not effected after the addition of lithium salts [19]. Fig. 5 (a) and (b) show symmetrical stretching mode of MG49 ether group,  $\nu_s(\text{C-O-C})$  at 986 cm<sup>-1</sup>. With the presence of LiClO<sub>4</sub> and LiBF<sub>4</sub>, the intensity of  $\nu_s(\text{C-O-C})$  in MG49-SnO<sub>2</sub> has been shifted to 984 cm<sup>-1</sup> and 991 cm<sup>-1</sup>, respectively. The vibration at stretching mode of -COO-,  $\nu(\text{C-O})$  at 1271 cm<sup>-1</sup> for MG49-SnO<sub>2</sub> has been shifted with the presence of LiClO<sub>4</sub> and LiBF<sub>4</sub> to 1281 cm<sup>-1</sup> and 1280 cm<sup>-1</sup>, respectively. Fig. 5 (a) and (b) also show asymmetrical stretching mode of ether group,  $\nu_{as}(\text{C-O-C})$  at 1147 cm<sup>-1</sup> for LiClO<sub>4</sub> and LiBF<sub>4</sub>. With the presence of 20% wt. LiClO<sub>4</sub> and LiBF<sub>4</sub>, the intensity of  $\nu_{as}(\text{C-O-C})$  in MG49-SnO<sub>2</sub> has been shifted to 1152 cm<sup>-1</sup> and 1151 cm<sup>-1</sup>, respectively. At the presence of 30% wt. LiClO<sub>4</sub> and LiBF<sub>4</sub>, the intensity of  $\nu_{as}(\text{C-O-C})$  shoulder at 1065 cm<sup>-1</sup> in MG49-SnO<sub>2</sub> has been shifted to 1071 cm<sup>-1</sup> and 1161 cm<sup>-1</sup>, respectively. The shifting on MG49-SnO<sub>2</sub>-LiBF<sub>4</sub> is about 6 cm<sup>-1</sup> to the higher wavenumbers due to the LiClO<sub>4</sub> peak at 1094 cm<sup>-1</sup> and about 4 cm<sup>-1</sup> to the lower wavenumbers LiBF<sub>4</sub> peak at 1027 cm<sup>-1</sup>. When the frequency of the infra-red spectrum is shifted to the left or lower wavenumbers, the interactions between the atoms are getting weaker due to the distraction that occurs on the molecule chain. The weakening of the polymeric chain is caused by nanosize ceramic fillers as reported by Chung et al [17]. The peak shift confirmed the interaction between lithium ion from doping salt and oxygen atoms in the structure of polymer host. This is because a new bond is formed between lithium ions from doping salt and oxygen atoms in the structure of polymer host to form a new bond called coordinate bond that leads to the formation of polymer-salt complexes [3].

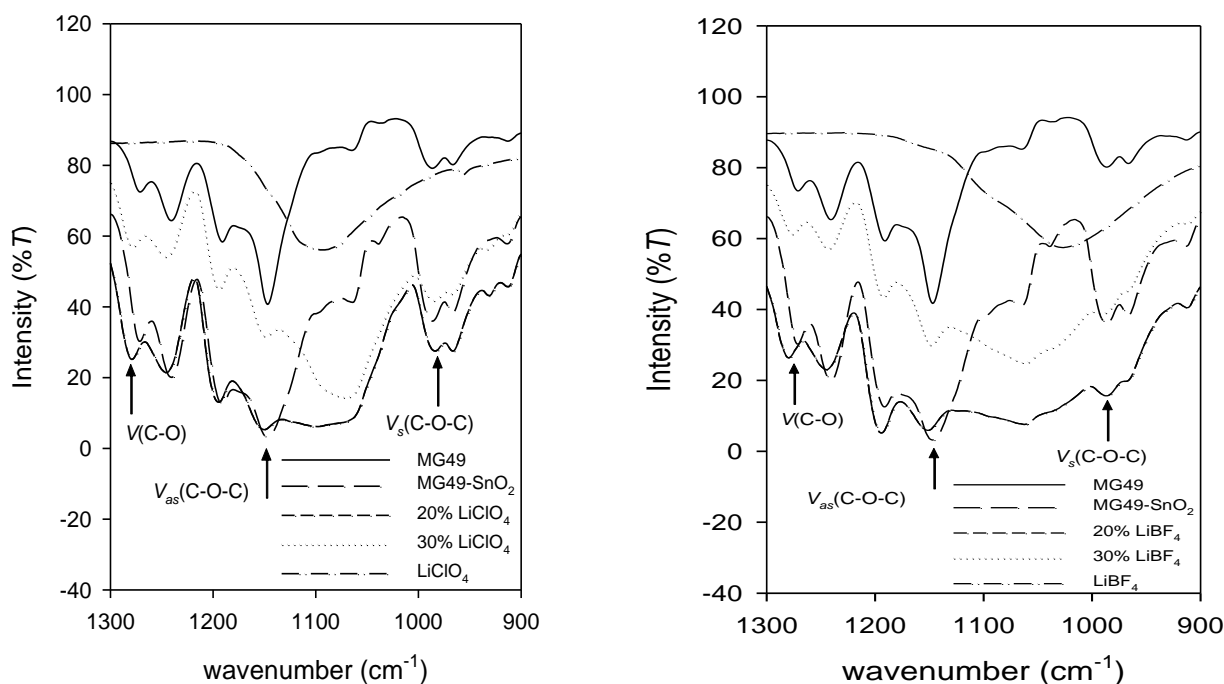


**Figure 5** FT-IR spectrum of asymmetrical stretching of ether group,  $\nu_{as}(\text{C-O-C})$  (a) LiClO<sub>4</sub> and (b) LiBF<sub>4</sub>

### 3.4 XPS Analysis

XPS spectroscopy is used to measure the elemental composition, chemical state and electronic state of the elements that exist on the surface of the polymer electrolytes. In development of lithium battery, the interaction between the electrolyte and the electrode would determine the performance of the battery. Therefore, surface analysis using XPS would be significant to spot the interaction occurred. Fig. 6 shows the XPS wide scan spectrum of SnO<sub>2</sub>, MG49, MG49-SnO<sub>2</sub>, MG49-SnO<sub>2</sub>-LiClO<sub>4</sub> and MG49-SnO<sub>2</sub>-LiBF<sub>4</sub>. All binding energy was corrected to C 1s peak corresponding to carbon in a hydrocarbon environment (CH<sub>x</sub>) at 284.5 eV [39]. The binding energy for Sn 3d<sub>5/3</sub> and Sn 3d<sub>3/2</sub> peak were observed at 487.4 eV and 495.9 eV, as similar to the previous finding [36,37,40.] This indicates that SnO or SnO<sub>2</sub> nanoparticles were present since they have a similar binding energy [36]. The binding of C 1s for carbonyl group (O=C-O-) and ether group (-C-O-) in MG49 pure was found at 288.6 eV and at 286.2 eV, respectively as shown in narrow scan spectrum in Fig. 7 (a).

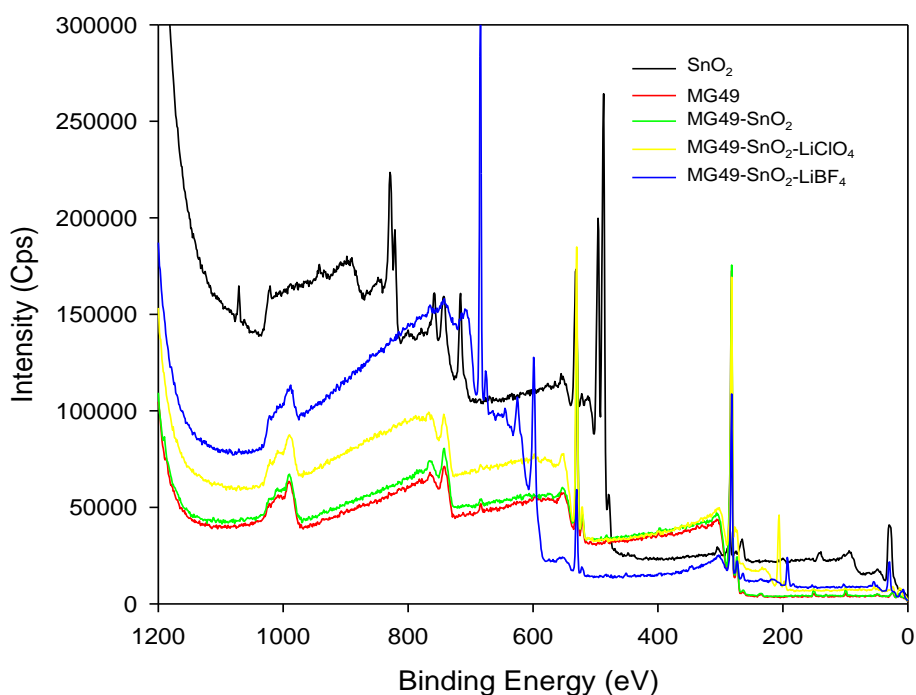


**Figure 6.** XPS wide scan spectrum of SnO<sub>2</sub>, MG49, MG49-SnO<sub>2</sub>, MG49-SnO<sub>2</sub>-LiClO<sub>4</sub> and MG49-SnO<sub>2</sub>-LiBF<sub>4</sub>

The O 1s main peak for SnO<sub>2</sub> was found at 531.3 eV as shown in Fig. 7 (b), which is close to the latest finding by Haverkamp et al. [40]. The spectrum gives an oxidation state of -2 for the oxygen atoms with a shoulder at the main peak that can be deconvoluted into two main components. One of the components is due to the structural of oxygen (O 1s) from Sn-O-Sn and Sn-O-H bonds as reported elsewhere [19, 36]. They suggested that the small shoulder at ~532 eV may be attributed to oxygen in adsorbed hydroxyl groups. Meanwhile, the binding energy for O 1s shows two main peaks for carbonyl group (O=C- & O=C-O) at 531.8 eV and 533.3 eV for ester group (-COOC-) in MG49. Both

peaks are assigned to lattice energy of oxygen [36]. This finding was exactly similar to the finding by López et al [39].

Upon the addition of SnO<sub>2</sub> into MG49 system, the binding energy for O 1s for carbonyl group (O=C- & O=C-O) and ester group (-COOC-) was not changed. This signifies that there is no chemical interaction occurred between SnO<sub>2</sub> nanoparticles and modified rubber, MG49 as discussed in the FTIR analysis section. With the presence of LiClO<sub>4</sub>, binding energy for O 1s for carbonyl group (O=C- & O=C-O) and ester group (-COOC-) has changed to 531.4 eV and 532.9 eV, respectively. The significant change for carbonyl group (O=C- & O=C-O) were found to be outside the range of  $\pm 0.1$  eV and  $\pm 0.2$  eV for ester group (-COOC-) as reported by López et al [39]. The binding energy for O 1s in MG49-SnO<sub>2</sub>-LiBF<sub>4</sub> was found to have a more significant change in comparison to LiClO<sub>4</sub>. The binding energy for O 1s for carbonyl group (O=C- & O=C-O) and ester group (-COOC-) with the presence of LiBF<sub>4</sub> was found at 532.1 eV and 533.0 eV, respectively. The shift in binding energy confirmed that the chemical interaction occurred in the MG49-lithium salts system. This is because a new coordinate bond is formed between lithium ion from doping salt and oxygen atoms in the structure of polymer host. The coordinate bond, leads to the formation of polymer-salt complexes as discussed in FTIR analysis [3].

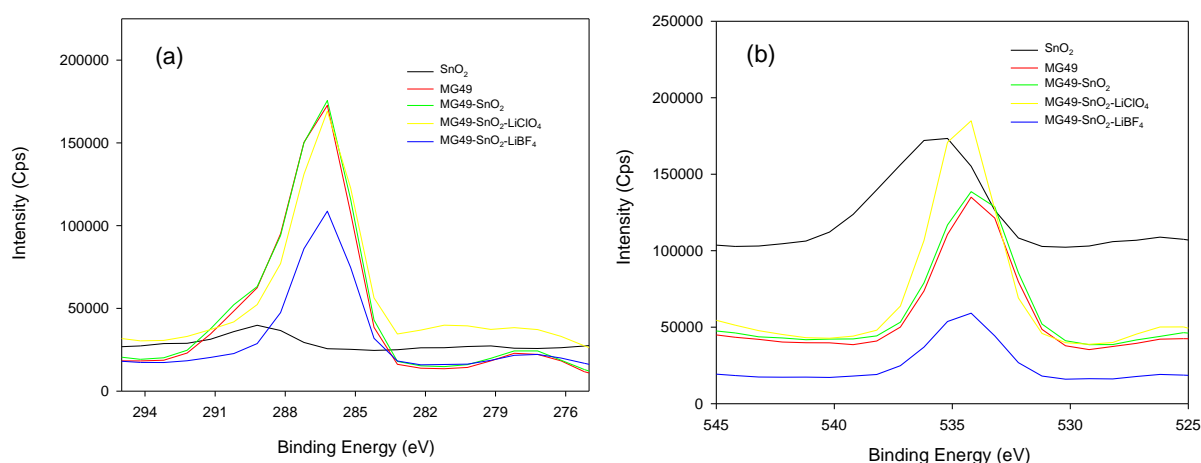


**Figure 7.** XPS narrow scan spectrum of (a) C 1s and (b) O 1s for MG49-SnO<sub>2</sub>-Lithium salts

### 3.5 Ionic conductivity

The typical impedance spectrum of MG49-SnO<sub>2</sub> with (a) 20% wt. LiClO<sub>4</sub> and (b) 30% wt. LiBF<sub>4</sub> are shown in Fig. 8. The complex impedance spectrum shows two well-defined regions; a semicircle in the high frequency range that is related to conduction process and the linear region in the low frequency range that is attributed to the bulk effect of blocking electrodes. In an ideal case at low frequency, the complex impedance plot shows a straight line parallel to the imaginary axis, but the double layer at blocking electrodes causes the curvature [41]. No charge will cross the electrodes from the dielectric material for blocking contacts and vice versa. The behaviour of dielectrics under the application of steady voltage depends mainly on the type of contacts between the electrodes and the

dielectric material. Therefore, in polymer electrolytes system the observed transient current will be due to the hopping process of positive and/or negative charges or both as reported elsewhere [28, 42, 43].

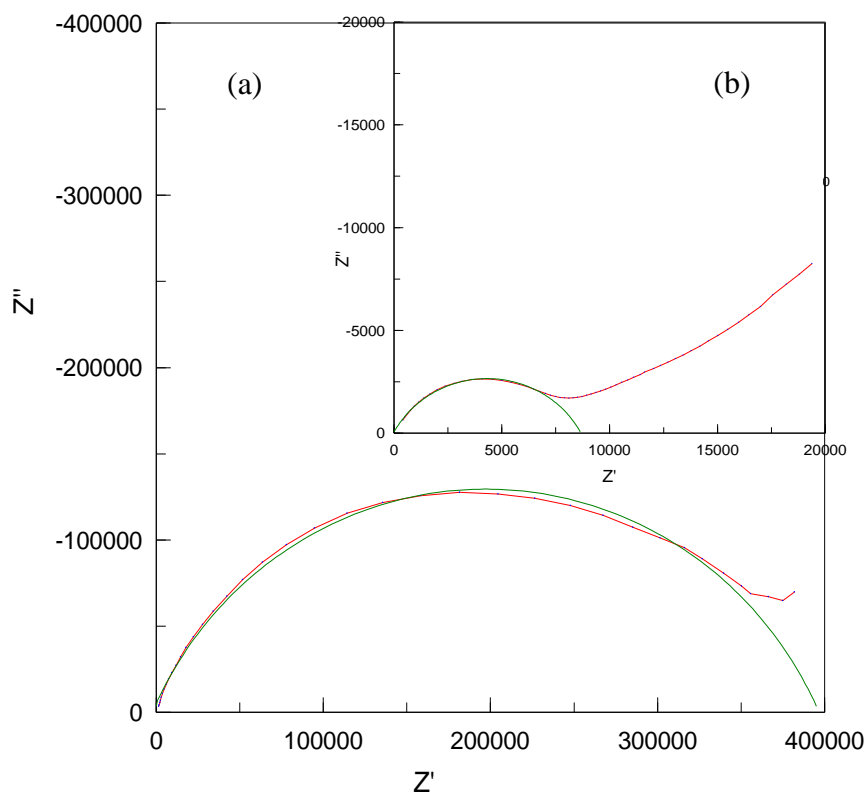


**Figure 8.** Impedance plot of MG49-SnO<sub>2</sub> with (a) 20% wt. LiClO<sub>4</sub> and (b) 30% wt. LiBF<sub>4</sub>

Ionic conductivity of MG49-SnO<sub>2</sub>-lithium salts is shown in Table 1. The ionic conductivity ( $\sigma$ ) was calculated from the bulk resistance ( $R_b$ ) that was obtained from the intercept on real impedance axis ( $Z'$  axis), the film thickness ( $l$ ) and contact area of the thin film ( $A = \pi r^2 = \pi (1.60 \text{ cm}/2)^2 = 2.01 \text{ cm}^2$ ), according to the equation  $\sigma = [l / (A \times R_b)]$ . Ionic conductivity without salt content is  $5.1 \times 10^{-10} \text{ S cm}^{-1}$ . The presence of 4% wt. SnO<sub>2</sub> nanoparticles increase the conductivity up to two magnitudes in comparison to previous studies on MG49 [11]. The ionic conductivity was found to increase as the lithium salt addition increases up to its maximum level. This is due to the increase of the lithium salt concentration that contributes to ion dissociation of ionic species [25]. The highest conductivity of MG49-SnO<sub>2</sub>-LiBF<sub>4</sub> is  $1.6 \times 10^{-6} \text{ S cm}^{-1}$  at 30% wt. LiBF<sub>4</sub>. Whereas, MG49-SnO<sub>2</sub>-LiClO<sub>4</sub> salts gives rise to  $6.0 \times 10^{-7} \text{ S cm}^{-1}$  at 20% wt. Higher ionic conductivity values are obtained in comparison to our previous studies on MG49 at the same salts concentration [11]. The conductivity of LiBF<sub>4</sub> system is close to that reported by Low et al. [15]. They found that the conductivity for MG49 system with the presence of 4% wt. TiO<sub>2</sub> poses the conductivity of  $1.1 \times 10^{-6} \text{ S cm}^{-1}$  at 30% wt. LiBF<sub>4</sub>. This indicates a wide band gap of SnO<sub>2</sub>,  $E_g = 3.6 \text{ eV}$  is not the key factor for enhancing the ionic conductivity [36]. From our previous works on MG49 [11] and MG49-PMMA [6] solid polymer electrolyte, LiBF<sub>4</sub> gives a higher ionic conductivity in comparison to LiClO<sub>4</sub> because of the difference in anion size that affects

the solubility of the salts. The atomic radius ( $r$ ) was calculated by Makoto Ue [23] using the Van Der Waals volume of each ion in accordance to the following equation:  $r = (3V/4\pi)^{1/3}$ . In that study, the atomic radius for  $\text{BF}_4^-$  was found to be 0.218  $r/\text{nm}$  in comparison to  $\text{ClO}_4^-$  at 0.215  $r/\text{nm}$ . The large anion size is required for delocalization of ionic charge that could minimize the lattice energy. Thus, this affects the solubility of the salts. The smaller cation size of lithium ion could contribute to the increase of ion dissociation resulted from the coulombic interaction forces between lithium cation and large anion. In addition,  $\text{BF}_4^-$  anion possesses high ionic mobility even though it has low dissociation constant [23]. This is generally expected to promote greater dissociation of salts; thus, provides a higher concentration of ions to mobile [14] Takami et al. [24] suggested that the lithium-ions batteries using the  $\text{LiBF}_4$  salts give an excellent performance and the most promising rechargeable battery with high energy density, high discharge performance, very low swelling for high-temperature storage and has excellent safety.

**Table 1.** Ionic conductivity of MG49-SnO<sub>2</sub>-lithium salt at room temperature

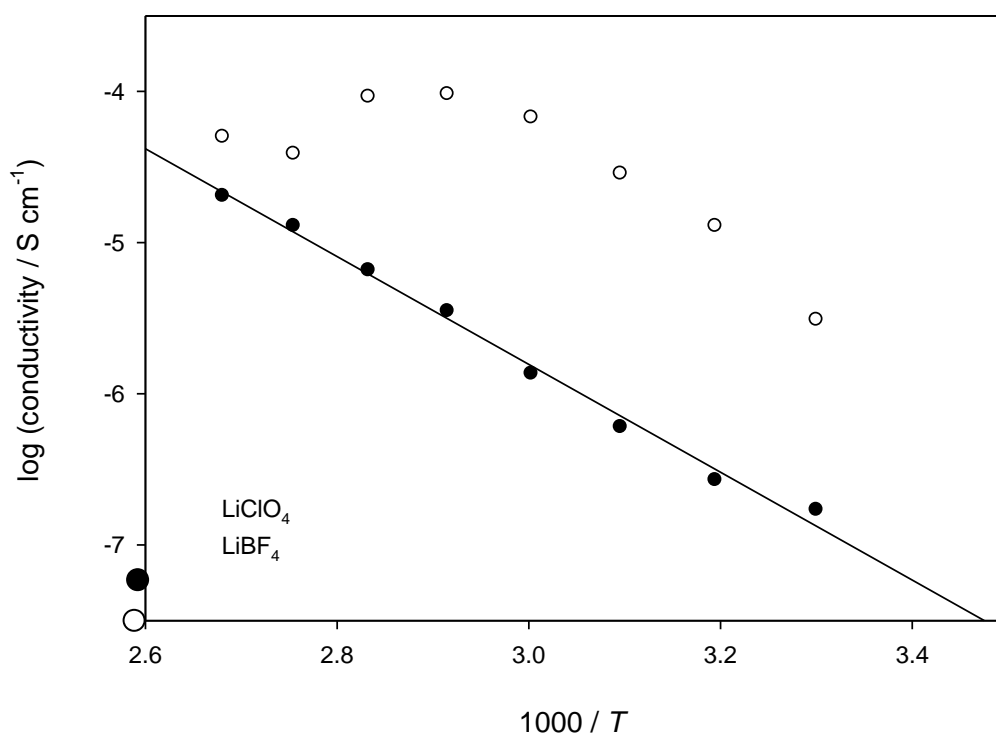
Sample	LiClO <sub>4</sub>	LiBF <sub>4</sub>
	Conductivity, $\sigma$ (S cm <sup>-1</sup> )	Conductivity, $\sigma$ (S cm <sup>-1</sup> )
0% wt.	$5.7 \times 10^{-10}$	$5.7 \times 10^{-10}$
5% wt.	$1.3 \times 10^{-9}$	$4.2 \times 10^{-10}$
10% wt.	$2.1 \times 10^{-9}$	$4.7 \times 10^{-10}$
15% wt.	$8.0 \times 10^{-9}$	$1.5 \times 10^{-9}$
20% wt.	$6.0 \times 10^{-7}$	$4.5 \times 10^{-8}$
25% wt.	$1.5 \times 10^{-8}$	$4.5 \times 10^{-7}$
30% wt.	$7.0 \times 10^{-9}$	$1.6 \times 10^{-6}$

Fig. 9 shows the temperature dependence of conductivity by the Arrhenius plot for the MG49-SnO<sub>2</sub> with 20% wt. LiClO<sub>4</sub> and 30% wt. LiBF<sub>4</sub> salts, respectively. It was observed that the conductivity increased with the temperature from 303 K to 373 K. The highest ionic conductivity for LiClO<sub>4</sub> was  $2.0 \times 10^{-5}$  S cm<sup>-1</sup> at 373 K and for LiBF<sub>4</sub> was  $9.4 \times 10^{-5}$  S cm<sup>-1</sup> at 343 K. The bulk resistance of the electrolyte is unobservable after 373 K since the sample was unstable at temperatures higher than 373 K. The relationship between conductivity and temperature for MG49-SnO<sub>2</sub>-LiClO<sub>4</sub> was found to be linear with the regression line of 0.9940. This indicates that the electrolyte system exhibited Arrhenius-like behaviour given by Arrhenius equation:  $\sigma = \sigma_0 e^{(-E_a/kT)}$ , where  $\sigma_0$ ,  $E_a$  and  $k$  represent the pre-exponential factor, activation energy and Boltzmann constant ( $k = 8.6 \times 10^{-5}$  eV K<sup>-1</sup>), respectively [5,6]. The value for  $\sigma_0$  and  $E_a$  is calculated from the y-axis and plot intercept between  $\log \sigma$  and  $1000/T$  [44].  $-E_a/kT$  is represented by the graph slope,  $m$ . From the Arrhenius plot, the activation energy,  $E_a$  is 0.25 eV. The pre exponential factor  $\sigma_0$  is  $5.33 \times 10^{-2}$  S cm<sup>-1</sup>. However, the pre-exponential factor  $\sigma_0$  and activation energy  $E_a$  of MG49-SnO<sub>2</sub>-LiBF<sub>4</sub> cannot be estimated from the plot because it was non-linear, which means its exhibited non-Arrhenius-like behaviour. Non-Arrhenius-like behaviour was associated with dynamic temperature dependence restructuring of the anion “sub-lattice” as explained by Kincs and Martin [45]. The non-Arrhenius-like behaviour was corresponding to ion transport in

polymer electrolytes is dependent on the segmental motion of the polymer [32]. Thus, the results may be effectively represented by the empirical Vogel–Tamman–Fulcher (VTF) equation based on the free volume concept:

$$\sigma = AT^{-1/2} \exp[-B/T-T_0]$$

where  $A$  and  $B$  are constants,  $T$  is the temperature in Kelvin (K) and  $T_0 = (T_g - 50)$ , the temperature taken 50 K below the glass transition temperature ( $T_g$ ). Constant  $A$  in the VTF equation is related to the number of charge carriers in the electrolyte system, and constant  $B$  is related to the activation energy of ion transport associated with the configurational entropy of the polymer chains [6,32].



**Figure 9.** Arrhenius plot for the MG49-SnO<sub>2</sub>-LiClO<sub>4</sub> and MG49-SnO<sub>2</sub>-LiBF<sub>4</sub>

### 3.6 Cyclic voltammetry

Cyclic voltammetry (CV) is one of the most commonly used electrochemical techniques to observe the electrochemical stability of the polymer electrolytes, in terms of electrochemical potential window. It is based on a linear potential waveform; which the potential is changed as a linear function of time. The electrochemical stability is an important parameter to be evaluated from the application point of view in electrochemical devices, such as batteries, supercapacitors, solar cell etc [46]. Fig. 10 shows comparative cyclic voltammograms of MG49-SnO<sub>2</sub> (4% wt.) with (a) 20% wt. LiClO<sub>4</sub> and (b) 30% wt. LiBF<sub>4</sub> at a scan rate of 5 mVs<sup>-1</sup>. The cathodic and anodic peaks are not distinctly

observed because the cell comprised of only the polymer electrolytes sandwiched between the symmetrical stainless steel electrodes due to instrument incompetent accessories [47]. The highest conductivity of composite polymer electrolyte has been used as initial indicator of the electrochemical stability. The electrochemical stability of MG49-SnO<sub>2</sub>-LiClO<sub>4</sub> has been found to maintain its shape even after the 100<sup>th</sup> cycle in the range of -2.0 to +2.2 mV and -8.0 to +6.0 mV for MG49-SnO<sub>2</sub>-LiBF<sub>4</sub>. The 100<sup>th</sup> cycle voltammogram deviates from the first shape due to ohmic drop [48].

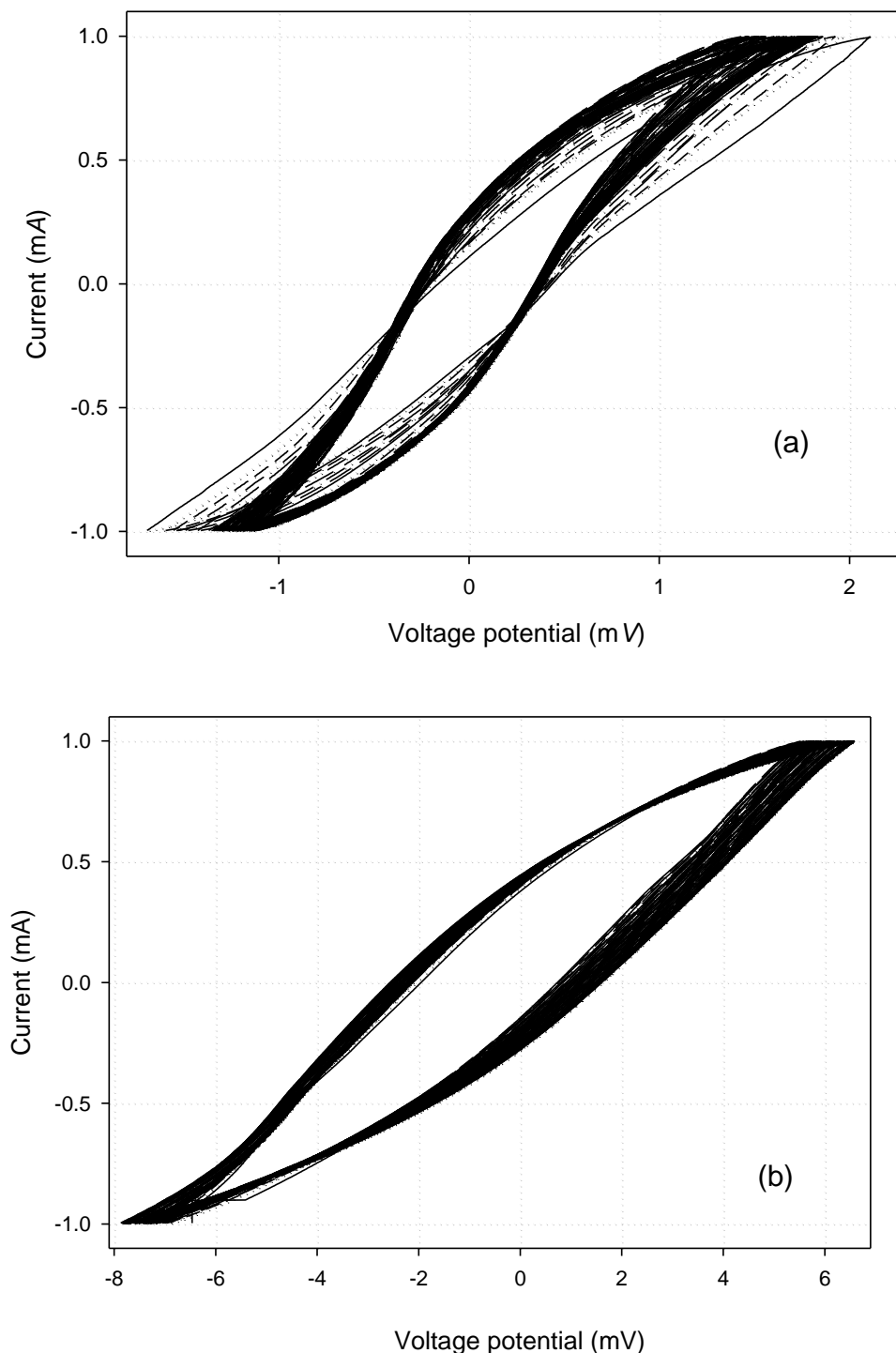


**Figure 10.** Voltammogram of MG49-SnO<sub>2</sub> with (a) 25% wt. LiClO<sub>4</sub> and (b) 30% wt. LiBF<sub>4</sub>

#### 4. CONCLUSIONS

Composite polymer electrolyte MG49-SnO<sub>2</sub> doped with two different lithium salts, LiClO<sub>4</sub> and LiBF<sub>4</sub> has been successfully prepared by solution casting technique. The highest conductivity achieved was around  $\sim 10^{-6}$  S cm<sup>-1</sup> at 30% wt. LiBF<sub>4</sub>, which was one order of magnitude higher in comparison to ionic conductivity found in the LiClO<sub>4</sub> system and two orders of magnitude higher in contrast to previous studies on MG49 based solid polymer electrolyte. This is due to the differences in anionic size and lattice energy of appropriate salt. Infrared and XPS analysis showed that the interaction between lithium ions and oxygen atoms occurred at carbonyl (C=O) and ether (C-O-C) group. Chemical analysis shows an important result of the SnO<sub>2</sub> filler does not interact with polymer or lithium salts. This observation is strengthening by SEM studies that show incompatibility between the SnO<sub>2</sub> filler and polymer matrix. The structural analysis recorded by XRD showed the semi-crystallinity phase of PMMA grafted natural rubber has reduced at highest conductivity. The electrochemical stability shows the possibility of MG49 based electrolytes to be fabricated in electrochemical devices.

#### ACKNOWLEDGEMENTS

The authors would like to extend their gratitude towards Universiti Kebangsaan Malaysia and Nuclear Malaysia for allowing this research to be carried out. We would like to extend our appreciation towards Prof. Dr. Alain Dufresne, Grenoble Institute of Technology, France for reviewing our draft manuscripts. Also, to Gamry instrument for the opportunity of using their cyclic voltammetry measurement. Last but not least, we would like to acknowledge all of the supports that have been given throughout the process of this manuscript. This Project has been funded by undergraduate allocation provided by the School of Chemical Sciences and Food Technology, UKM.

#### References

1. D.E. Fenton, J.M. Parker and P.V. Wright, *Polymer*, 14 (1973) 589.
2. F.M. Gray, *Polymer Electrolytes, Material Monographs*, (1987) RSC, London.
3. K. Kumutha and Y. Alias, *Spectrochim Acta Part A*, 64 (2006) 442.
4. A.M.M. Ali, R.H.Y. Subban, H. Bahron, T. Winie, F. Latif and M.Z.A. Yahya, *Ionics*, 14 (2008) 491.
5. S.A.M. Noor, A. Ahmad, I.A. Talib and M.Y.A. Rahman, *Ionics*, 16 (2010) 161.
6. M.S. Su'ait, A. Ahmad, H. Hamzah and M.Y.A. Rahman MYA, *Electrochim Acta*, 57 (2011) 123.
7. R. Idris, M.D. Glasse, R.J. Latham, R.G. Linford and W.S. Schlindwein, *J Power Sources*, 94 (2000) 206.
8. M.D. Glasse, R. Idris, R.J. Latham, R.G. Linford and W.S. Schlindwein, *Solid State Ionics*, 147 (2002) 289.
9. F. Latif, A.M. Aziz, N. Katun, A.M.M. Ali and M.Z.A. Yahya MZA (2006) *J Power Sources*, 159 (2006) 1401.
10. S.A.M. Noor, A. Ahmad, I.A. Talib and M.Y.A. Rahman, *Ionics*, 17 (2011) 451.
11. M.S. Su'ait, A. Ahmad, H. Hamzah and M.Y.A. Rahman, *Ionics*, 15 (2009) 497.
12. M.S. Su'ait, A. Ahmad, H. Hamzah and M.Y.A. Rahman, *J Phys D*, 42 (2009) 055410.
13. A. Ahmad, P.C. Lien and M.S. Su'ait, *Sains Malaysiana*, 39 (2010) 65.
14. Y. Alias, I. Ling and K. Kumutha, *Ionics*, 11 (2005) 414.

15. S.P. Low, A. Ahmad, H. Hamzah and M.Y.A. Rahman, *J Solid State Electrochemistry*, 15 (2011) 2611.
16. S.P. Low, A. Ahmad and M.Y.A. Rahman, *Ionics*, 16 (2010) 821.
17. S.H. Chung, Y. Wang, L. Persi, F. Croce, S.G. Greenbaum, B. Scrosati and E. Plichta, *J Power Sources*, 97 (2001) 644.
18. P.V.S. da Conceição, L.O. Faria, A.P. Santos and C.A. Furtado, *MRS Proceedings*, 756 (2002) DOI:10.1557/PROC-756-EE3.14.
19. H.M. Xiong, K.K. Zhao, X. Zhao, Y.W. Wang and J.S. Chen, *Solid State Ionics*, 159 (2003) 89.
20. A. Loupy and B. Tchoudar B, *Salts Effects in Organic and Organic Metallic Chemistry*, (1991) VCH Publishing, New York.
21. Y. Xinhe, C.J., Li and W. Wang, *Acta Polymerica Sinica*, 2 (1998) 139.
22. K. Xu, *Chem Rev*, 104 (2004) 4303.
23. M. Ue, *Electrochim. Acta*, 39 (1994) 2083.
24. N. Takami, M. Sekino, T. Ohsaki, M. Kanda and M Yamamoto, *J Power Sources*, 97-98 (2001)677.
25. K. Kumutha, Y. Alias and R. Said, *Ionics*, 11 (2005) 472.
26. A. Ahmad, M.Y.A. Rahman and M.S. Su'ait, *Physica B*, 403 (2008) 4128.
27. E.Z. Monikowska, Z. Florajmczyk, E.R. Jonska, A. Werbanowska, A. Tomaszewska, N.Langwald, D. Golodnitsky, E. Peled, R. Korvarsky, S.H. Chung and S.G. Greenbaum, (2007) *J Power Sources*, 173 (2007)734.
28. Y.G. Andreev and P.G. Bruce, *Electrochim Acta* 45 (2000) 1417.
29. A. Ahmad, M.Y.A. Rahman, M.L.M. Ali, H. Hashim and F.A. Kalam, *Ionics*, 13 (2007) 67.
30. J.R. Wickham, R.N. Mason and C.V. Rice, *Solid State Nucl Magn Reson*, 31 (2007) 184.
31. R.H.Y. Subban and A.K. Arof, *J New Mater Electrochem Syst*, 6 (2003) 197.
32. S. Rajendran, T. Uma and T. Mahalingam, *Ionics*, 5 (1999) 232.
33. A.M.M. Ali, M.Z.A.Yahya, H. Bahron and R.H.Y. Subban, *Ionics*, 12 (2006) 303.
34. R. Baskaran, S. Selvasekarapandian, N. Kuwata, J. Kawamura and T. Hattori, *Solid State Ionics*,177 (2006) 2679.
35. O. Mahendran and S. Rajendran, *Ionics*, 9 (2003) 282.
36. P. Stefanov, G. Anatasova, E. Manolov, Z. Raicheva and V. Lazarova, *J Phys:Conf Ser*, 100 (2008) 082046.
37. Z. Li, Q. Zhao, W. Fan and J. Zhan, *Nanoscale*, 3 (2011) 1646.
38. D.L. Pavia, G.M. Lampman and G.S. Kriz, *Introduction to spectroscopy*, (2001) Brooks/Cole Publishing, USA.
39. G.P. López, D.G. Castner and B.D. Ratner, *Surf Interface Anal*, 17 (1991) 267.
40. R.G. Haverkamp, A.T. Marshall and B.C.C. Cowie, *Surf Interface Anal*, 43 (2011) 847.
41. C. Kim, G. Lee, K. Liou, K.S. Ryub, G.K. Seong and S.H. Chang, *Solid State Ionics*, 123 (1999) 251.
42. S.F. Potamianou, K.A.T. Thoma and M.N. Pisanias, *J Phys A*, 23 (1990) 1313.
43. J. Spěvácěk, J. Brus and J. Dybal, *Solid State Ionics*, 176 (2005) 163.
44. L. Othman, K.W. Chew and Z. Osman, *Ionics*, 13 (2007) 337.
45. J. Kincs and S.W. Martin, *Phys. Rev. Lett.*, 76 (1996) 70.
46. G.P. Pandey, Y. Kumar and S.A. Hashmi, *Solid State Ionics*, 190 (2011) 93.
47. Y. Kumar, S.A. Hashmi and G.P. Pandey, *Electrochim Acta*, 56 (2011) 3864.
48. S.N. Asmara, M.Z. Kufian, S.R. Majid and A.K. Arof, *Electrochim Acta*, 57 (2011) 91.